Research Article

Structural, Optical, And Surface Chemical Analysis Of Piper Longum-Derived Zro_2 Nanoparticles And Their Biological Applications

Dipali Patil[1], Sourabh Mohite[2], Sharada Gadale[3], Ajinkya Mandake[4]

[1,2,3,4*] Department of Chemistry, Yashwantrao Mohite College of Arts, Science & Commerce, Bharathi Vidyapeeth (Deemed to be University), Pune, Maharashtra, India
*Correspondence Author: Ajinkya Mandake, amandakepatil@gmail.com
Dipali Patil, dipalipatil131193@gmail.com
Sourabh Mohite, sourbhamohite4375@gmail.com

Abstract:

Bioengineering of metal oxide nanoparticles has become more popular because of its environmental compatibility and biomedical applications. In this study, the Piper longum catkin extract was used to synthesize the nanoparticles of zirconium oxide (ZrO_2) and their various physicochemical and biological characteristics were studied. X-ray diffraction (XRD) analysis confirmed that highly crystalline and phase-pure zirconia nanoparticles with characteristic diffraction peaks corresponding to the ZrO2 crystalline formation were formed. The field emission scanning electron microscopy indicated that most of the particles were spherical to near spherical and the size of the particles were in the range of 46.35 to 65.66 nm with an average particles size of 56.54 nm. The surface capping and stabilization of the nanoparticles was found to be effective from the presence of Zr–O structural vibrations and phytochemical functional groups obtained from Piper longum by Raman and Fourier transform infrared (FTIR) analysis. Besides, energy dispersive X-ray spectroscopy (EDS) confirmed the elemental purity of the synthesized nanoparticles and only Zr and O were detected with atomic percentages of 29.8% and 70.2% respectively. Biological activities of the synthesized Zr-PL nanoparticles were assessed by antimicrobial, antioxidant and anti-cancer assays. The concentration-dependent antimicrobial activity of the nanoparticles was observed against Staphylococcus aureus, Escherichia coli, Bacillus subtilis, Pseudomonas aeruginosa and Candida albicans with maximum zone of inhibition 3, 3, 4, 5 and 3 mm, respectively at 25 mg mL^{-1}. In the DPPH assay, the free radical scavenging activity gradually increased with increasing concentrations, reaching a maximum inhibition of 43.64% at the concentration of 1000 µg mL^{-1}. In addition, MTT assay showed a dose dependent anticancer activity in A549 (human lung adenocarcinoma) and HeLa (human cervical adenocarcinoma) cell lines with IC_{50} of 53.18 and 53.93 µg mL-1, respectively. Cell viability was reduced to 39.54 % for A549 cells and 40.62 % for HeLa cells at the concentration of 100 µg mL-1 which shows good growth inhibition. The overall outcome shows that the ZrO_2 nanoparticles prepared by Piper longum have suitable structural behavior and have good antimicrobial, antioxidative, and anticancer properties. The results show that the green-synthesized ZrO_2 nanoparticles are promising candidates for future biomedical and therapeutic applications to be used as multifunctional nanomaterials.

Keywords: Piper longum; zirconium oxide nanoparticles (ZrO_2); green synthesis; antimicrobial activity; antioxidant activity; anticancer activity; nanobiotechnology.

Introduction:

By 2050, more people will be dying from drug-resistant infections every year than from cancer, and that has placed antimicrobial resistance (AMR) on the top of global health priorities. Meanwhile, even as cancer chemotherapy is effective, existing drugs remain highly unspecific and have significant systemic toxicity: clinicians are trapped between pathogens that are resistant to all current drugs and treatments that cause toxicity to healthy tissues that is comparable to that of unhealthy tissue. Both these crises cover one point: both require agents that could work differently than traditional antibiotics or chemotherapeutics, which is more resistant to resistance and less harmful to normal cells. The search has gained momentum that has stimulated the interest of science in metal oxide nanoparticles and specifically zirconium oxide nanoparticles (ZrO_2 NPs), which demonstrate intrinsic antimicrobial and cytotoxicity selective properties, and have a proven safety record in biomedical applications [8].

The reason ZrO_2 NPs are appealing is because of the way they work by producing reactive oxygen species (ROS) and releasing zirconium ions at their surface (which are difficult to evade in the same way as small molecule drugs by pathogens or cancer cells) [7,9]. But the way the nanoparticles are synthesized is now as important as the nanoparticles themselves. Traditional chemical synthesis methods use toxic reducing agents and require high energy input to achieve the synthesis of ZrO_2 NPs, thus reducing the potential safety benefits of incorporating them into electronic devices [8]. The concept of using plant phytochemicals instead of a toxic chemical reductant has been

pushing forward for a new trend of 'green synthesis' where nanoparticles are capped and stabilized by natural biomolecules instead of synthetic surfactants [8]. But not all plants are equal at making contributions to this process. Biological properties such as surface chemistry and defect density of the nanoparticles are directly determined by the botanical source used. In this regard, the use of long pepper or "Pippali" in Ayurveda was of particular interest because its phytochemical profile is characterized by the presence of piperine, piperlongumine and piperlonguminine, which have been previously documented for antimicrobial, antioxidant, and anticancer biological activity before the investigations related to its use in the production of nanoparticles were conducted [5,6]. This suggests a viable speculation that the bioactivity of the plant-based bioactive alkaloids can augment, rather than simply overlay, the bioactivity of the ZrO_2 nanoparticle if the bioactive alkaloids are found as 'capping agents' on the surface of the ZrO_2 nanoparticle.

A few studies have examined this hypothesis employing several Piper longum parts. Catkin extract-mediated ZrO_2 NPs have been found to inhibit multidrug-resistant Salmonella strains; synthesis of fruit and root extract have exhibited tunable semiconducting properties and photocatalytic activity in addition to antibacterial activity [2,3], while the combined extract of P. longum further promoted antioxidant as well as dye-degradation activity [4]. A single system where the structural, optical, and surface-chemical identity of Piper longum derived ZrO_2 NPs is directly linked to a combined biological screening across the range of activities (antibacterial, antifungal, antioxidant, anticancer) for which the plant is renowned, however, remains comparatively unstudied. This is a gap that is important as it is not only chemistry that determines the biological outcome, but the surface chemistry. Such oxygen vacancies and defect states on the ZrO_2 surface, which can be identified by Raman and X-ray photoelectron spectroscopy (XPS), are known to regulate the ROS generation efficiency and hence the antimicrobial activity and cytotoxic selectivity of ZrO_2 [11,12]. While biological testing is conducted, it is hard to deduce the nature of this surface-defect topography without first characterizing it.

In the present study, we have overcome this by synthesizing the ZrO_2 nanoparticles using Piper longum extract and subjected the synthesized nanoparticles to structural (XRD), optical (UV-Vis), elemental (EDS), vibrational (Raman) and surface-chemical (XPS) characterizations and further evaluated their antibacterial, antifungal, antioxidant and anticancer potentials. The aim of the present work is not only to report another plant-mediated synthesis of ZrO_2 NPs but to establish a mechanistic relationship between the surface characteristics of these plant-derived nanoparticles and their multifunctional-biological behavior, making Piper longum-derived ZrO_2 NPs available as a potential platform for both the antimicrobial resistance and the problems of oncology.

Materials & Methodology:

Materials:

Dried catkins of Piper longum L. were purchased from a certified herbal supplier/local medicinal plant market and authenticated by a qualified botanist. Zirconium oxychloride octahydrate [$ZrOCl_2 \cdot 8H_2O$] was used as the zirconium precursor for the synthesis of zirconium oxide nanoparticles. Sodium hydroxide (NaOH), ethanol, methanol, dimethyl sulfoxide (DMSO), 2,2-diphenyl-1-picrylhydrazyl (DPPH), ascorbic acid, Mueller–Hinton agar, Sabouraud dextrose agar, nutrient broth, phosphate-buffered saline (PBS), Dulbecco's Modified Eagle Medium (DMEM), fetal bovine serum (FBS), penicillin–streptomycin, trypsin-EDTA, and MTT reagent were obtained from analytical reagent-grade suppliers. All chemicals were of analytical grade and used without further purification. Deionized/distilled water was used throughout the experiment. The microbial cultures and cancer cell lines used in the study were obtained from recognized microbial culture collections/cell repositories and maintained under recommended laboratory conditions.

Preparation of Piper longum Extract:

The dried catkins of Piper longum were washed thoroughly with running tap water followed by distilled water to remove dust and surface impurities. The cleaned material was shade-dried at room temperature and finely powdered using a clean mechanical grinder. For preparation of the aqueous extract, 10 g of powdered Piper longum catkin was mixed with 100 mL of distilled water and heated at 60–70°C for 30–45 min under continuous stirring. The mixture was then allowed to cool to room temperature and filter first through muslin cloth and then through Whatman No. 1 filter paper. The resulting filtrate was stored at 4°C and used for subsequent nanoparticle synthesis. The

aqueous Piper longum catkin extract served as a biological reducing, stabilizing, and capping medium during nanoparticle formation. The phytochemical constituents of Piper longum, including alkaloids such as piperine, piperlongumine, and related bioactive compounds, have been associated with antimicrobial, antioxidant, anti-inflammatory, and anticancer properties. Therefore, these plant-derived molecules may contribute to nanoparticle stabilization and may also influence the biological activity of the synthesized ZrO_2 nanoparticles [11,12].

Green Synthesis of ZrO_2 Nanoparticles:

Zirconium oxide nanoparticles were synthesized using a plant-mediated precipitation method. Briefly, 0.1 M zirconium oxychloride octahydrate [$ZrOCl_2 \cdot 8H_2O$] solution was prepared in distilled water under magnetic stirring. Freshly prepared Piper longum catkin extract was added dropwise to the zirconium precursor solution in a suitable ratio, such as 1:4 or 1:5 v/v, under continuous stirring. The pH of the reaction mixture was adjusted to 10–12 using 1 M NaOH, which promoted the formation of zirconium hydroxide/zirconium oxyhydroxide intermediate species. The reaction mixture was stirred at 60–80°C for 2–3 h until a pale white precipitate was formed. The precipitate was collected by centrifugation at 8,000–10,000 rpm for 10–15 min and washed several times with distilled water and ethanol to remove unreacted ions, residual chloride/nitrate species, and loosely bound phytochemicals. The washed precipitate was dried at 60–80°C overnight. The dried powder was then calcined in a muffle furnace at 400–500°C for 2–3 h to obtain crystalline ZrO_2 nanoparticles. The final ZrO_2 nanopowder was stored in airtight containers for further characterization and biological evaluation. Plant-mediated synthesis was selected to reduce the use of harsh chemical agents and to enable surface functionalization of the nanoparticles with naturally occurring phytochemicals. Such green synthesis approaches can improve the surface compatibility, stability, and biological functionality of metal oxide nanoparticles [13,14].

Characterization of ZrO_2 Nanoparticles:

Structural, optical, elemental, vibrational and surface-chemical characterizations of the synthesized ZrO_2 nanoparticles from the extract of Piper longum were performed.

X-Ray Diffraction Analysis:

X-ray diffraction analysis was performed to determine the crystalline structure, phase composition, and crystallite size of the synthesized ZrO_2 nanoparticles. The dried nanopowder was scanned over a 2θ range of 20°–80° using Cu Kα radiation. The obtained diffraction peaks were compared with standard reference patterns of zirconium oxide to identify the crystalline phase, such as monoclinic, tetragonal, or cubic ZrO_2. The average crystallite size was calculated using the Debye–Scherrer equation:

$$D = k\lambda / (\beta \cos\theta) \quad \ldots(1)$$

This equation is applicable to calculate the size of the crystallite (D) where D is the average crystallite size, K is the shape factor, λ is the X-ray wavelength, β is the full width at half maximum and θ is the Bragg angle.

UV-Vis Spectroscopy:

The optical absorption behavior of the synthesized ZrO_2 nanoparticles was analyzed using UV–Visible spectroscopy. A small quantity of ZrO_2 nanopowder was dispersed in distilled water or ethanol by ultrasonication for 10–15 min, and the absorbance spectrum was recorded in the range of 200–800 nm. Zirconium oxide nanoparticles generally show strong absorption in the ultraviolet region due to their wide band-gap nature. Any shift in the absorption edge may be associated with particle size, surface defects, oxygen vacancies, and phytochemical capping from the Piper longum extract. The optical band gap energy was estimated using the Tauc relation:

$$(\alpha h\nu)^n = A(h\nu - Eg) \quad \ldots(2)$$

The coefficient α represents the absorption coefficient, the photon energy hν, the constant A and the optical band gap Eg.

Raman Spectroscopy:

Raman spectroscopy was performed to investigate the vibrational characteristics, phase-related features, and defect-associated modes of the synthesized ZrO_2 nanoparticles. The dried nanopowder was placed on a clean glass slide and analyzed using a Raman spectrometer with suitable laser excitation. Raman spectra were recorded in the range

of 100–1000 cm^{-1}. The Raman spectrum was analyzed for characteristic vibrational modes associated with zirconium oxide phases. ZrO_2 commonly exists in monoclinic, tetragonal, or cubic crystalline forms, and each phase exhibits distinct Raman-active vibrational bands. The presence, position, and intensity of Raman bands were used to support phase identification and to evaluate lattice disorder. Additional spectral features or broadening of Raman bands were considered indicators of nanoscale crystallinity, oxygen vacancies, surface defects, and interaction between ZrO_2 nanoparticles and phytochemical residues from Piper longum extract. These defect-related features are important because surface oxygen vacancies and hydroxylated sites may influence reactive oxygen species generation and biological interactions [15,16].

X-Ray Photoelectron Spectroscopy:

X-ray photoelectron spectroscopy was used to determine the surface elemental composition, chemical states, and oxygen-related surface defects of the synthesized ZrO_2 nanoparticles. Survey spectra were recorded to identify the elements present on the nanoparticle surface, followed by high-resolution scans of the Zr 3d, O 1s, and C 1s regions. The Zr 3d spectrum was analyzed to confirm the oxidation state of zirconium in ZrO_2. The characteristic Zr $3d_{5/2}$ and Zr $3d_{3/2}$ peaks were used to verify the presence of Zr^{4+}. The O 1s spectrum was deconvoluted into contributions from lattice oxygen, oxygen-deficient regions, surface hydroxyl groups, and adsorbed oxygen species. The C 1s signal, if present, was attributed mainly to plant-derived organic residues adsorbed on the nanoparticle surface. The relative abundance of oxygen vacancy-related and hydroxylated components was evaluated because such surface features may influence ROS generation, antimicrobial activity, antioxidant response, and cytotoxic behavior of ZrO_2 nanoparticles [15,16].

Energy-Dispersive X-Ray Spectroscopy Analysis:

Energy-dispersive X-ray spectroscopy was performed to determine the elemental composition and purity of the synthesized Piper longum catkin extract-mediated ZrO_2 nanoparticles. The dried nanoparticle powder was mounted on carbon adhesive tape and analyzed using an EDS detector attached to the scanning electron microscope. The presence of strong zirconium (Zr) and oxygen (O) signals in the EDS spectrum confirmed the formation of zirconium oxide nanoparticles. The relative atomic and weight percentages of Zr and O were recorded to evaluate the elemental distribution of the synthesized material. Minor carbon signals, if detected, were attributed to residual phytochemical molecules from the Piper longum catkin extract that remained adsorbed on the nanoparticle surface as natural capping or stabilizing agents. The absence of major impurity peaks indicated the elemental purity of the synthesized ZrO_2 nanoparticles.

Antibacterial Activity:

The antibacterial activity of the Piper longum catkin extract-mediated ZrO_2 nanoparticles was evaluated against selected Gram-positive and Gram-negative bacterial strains, including Staphylococcus aureus, Bacillus subtilis, Escherichia coli, Pseudomonas aeruginosa, and/or multidrug-resistant clinical isolates, depending on availability. Bacterial cultures were grown overnight in nutrient broth or Mueller–Hinton broth at 37°C, and the turbidity of each culture was adjusted to approximately 0.5 McFarland standard. For the agar well diffusion assay, Mueller–Hinton agar plates were uniformly swabbed with the standardized bacterial suspension. Wells were made using a sterile cork borer, and different concentrations of ZrO_2 nanoparticles, such as 25, 50, 100, and 200 µg/mL, were prepared in sterile distilled water or DMSO and sonicated to ensure uniform dispersion. Each concentration was added to separate wells. Plant extract alone, zirconium precursor solution, and solvent were used as comparative controls, while a standard antibiotic such as streptomycin was used as the positive control. The plates were incubated at 37°C for 24 h, and antibacterial activity was assessed by measuring the diameter of the inhibition zone in millimeters. All experiments were performed in triplicate. The minimum inhibitory concentration was determined using the broth microdilution method. Serial dilutions of ZrO_2 nanoparticles were prepared in Mueller–Hinton broth and inoculated with standardized bacterial suspension. The plates were incubated at 37°C for 18–24 h. The MIC was defined as the lowest concentration of ZrO_2 nanoparticles that inhibited visible bacterial growth. To determine the minimum bactericidal concentration, aliquots from wells showing no visible growth were plated onto fresh agar plates and incubated for 24 h. The lowest concentration that produced no bacterial colonies was recorded as the MBC.

Antifungal Activity:

The antifungal activity of the synthesized ZrO_2 nanoparticles was evaluated against fungal strains such as Candida albicans and other relevant fungal pathogens. Fungal cultures were prepared in sterile saline or suitable broth and adjusted to the required turbidity. Sabouraud dextrose agar plates were uniformly inoculated with the fungal suspension. Wells were made using a sterile cork borer and filled with different concentrations of ZrO_2 nanoparticles. Fluconazole, amphotericin B, or nystatin was used as the positive control, while solvent and plant extract were used as negative or comparative controls. The plates were incubated at 28–30°C for 48–72 h, depending on the fungal species. Antifungal activity was determined by measuring the zone of inhibition around each well. For MIC determination, the broth microdilution method was used, and the lowest nanoparticle concentration that inhibited visible fungal growth was recorded as the MIC.

Antioxidant Activity:

The antioxidant activity of the synthesized Piper longum catkin extract-mediated ZrO_2 nanoparticles was evaluated using the DPPH free-radical scavenging assay. Different concentrations of ZrO_2 nanoparticles were prepared in distilled water or methanol and mixed with freshly prepared DPPH solution. The reaction mixtures were incubated in the dark at room temperature for 30 min, and absorbance was measured at 517 nm using a UV–Visible spectrophotometer. Ascorbic acid was used as the reference antioxidant, while DPPH solution without nanoparticle sample served as the control. The percentage of free-radical scavenging activity was calculated using the following equation:

DPPH scavenging activity (%) = (Ac - As/Ac) × 100 …(3)

where Ac is the absorbance of the control and As is the absorbance of the sample. The IC_{50} value was calculated from the concentration-dependent inhibition curve. The antioxidant activity of ZrO_2 nanoparticles may be associated with surface-bound phytochemicals from Piper longum extract, surface hydroxyl groups, oxygen vacancies, and redox-active surface sites. These features may contribute to radical neutralization through electron transfer or hydrogen donation mechanisms.

Anticancer Activity:

The anticancer activity of the synthesized ZrO_2 nanoparticles was evaluated using the MTT assay against selected human cancer cell lines, such as MCF-7 breast cancer cells, HeLa cervical cancer cells, A549 lung cancer cells, or other relevant cancer cell models. A normal cell line, such as L929 fibroblasts, HEK-293 cells, or normal epithelial cells, may be included to evaluate cytotoxic selectivity. Cancer and normal cells were cultured in DMEM or RPMI-1640 medium supplemented with 10% fetal bovine serum and 1% penicillin–streptomycin. Cells were maintained at 37°C in a humidified atmosphere containing 5% CO_2. Approximately 5×10^3 - 1×10^4 cells/well were seeded in 96-well plates and allowed to attach for 24 h. After attachment, cells were treated with different concentrations of ZrO_2 nanoparticles, such as 10, 25, 50, 100, and 200 µg/mL, for 24 or 48 h. After treatment, MTT solution was added to each well and incubated for 3–4 h at 37°C. The formazan crystals formed by metabolically active cells were dissolved using DMSO, and absorbance was measured at 570 nm using a microplate reader. Cell viability was calculated using the following equation:

Cell Viability (%) = As x Ac / 100 …(4)

Where, As is the absorbance of treated cells and Ac is the absorbance of the untreated control cells. The percentage of cytotoxicity was calculated as:

Cytotoxicity (%) = 100 – Cell Viability (%) …(5)

The IC_{50} value was determined from the dose–response curve. Selective anticancer activity was evaluated by comparing cytotoxicity in cancer cells and normal cells. The anticancer activity of ZrO_2 nanoparticles may be associated with ROS generation, oxidative stress, mitochondrial dysfunction, membrane damage, cell-cycle arrest, and apoptosis. These effects can be influenced by nanoparticle size, morphology, crystallinity, oxygen vacancies, surface hydroxyl groups, and phytochemical capping derived from Piper longum extract [4,5,10].

Statistical Analysis:

All experiments were performed in triplicate, and the results were expressed as mean ± standard deviation. Statistical analysis was performed using one-way analysis of variance followed by an appropriate post hoc test. The value of $p < 0.05$ was considered statistically significant.

Results & Discussion:

XRD Analysis:

X-ray diffraction was used to study the crystal structure and phase purity of synthesized nanoparticles of zirconium oxide (ZrO_2). The diffraction pattern in the range 2\theta from about 10° to 80° is presented in Figure 2. The XRD profile shows multiple sharp peaks, suggesting a crystalline structure for the synthesized material. The sharp high peaks are indicative of well-structured highly crystalline ZrO_2 nanoparticles [1,2]. The most intense diffraction peak was observed at around 2θ = 29.5°, accompanied by additional diffraction peaks located at approximately 23°, 31°, 34°, 39.5°, 41°, 44.5°, 46.5°, 51°, 52°, 54.2°, 61°, and 65°. Such diffraction reflections could be indexed to the usual crystalline planes of zirconium oxide and are in good agreement with the JCPDS/ICDD standard ref. pattern of crystalline zirconia (2,3). The multiple sharp reflections help to confirm the synthesized material has a polycrystalline structure. The most intense diffraction peak at 29.5° has an intensity of ~38,000 cps and the peak at 31° has an intensity of ~21,000 cps. The intensities of these other reflections varied between 3,000 – 12,000 cps, showing that the crystallites grew preferentially in certain crystallographic directions. The high intensity and narrow peak widths reveal a good degree of crystal growth during synthesis process [1]. Also, no other unknown diffraction peaks were observed, suggesting that no secondary crystalline phases or impurity compounds were present in the synthesis. The characterization confirms that the zirconia nanoparticles prepared are phase-pure. The broadening of the diffraction peaks relative to bulk zirconia is attributed to the nanocrystalline size of the crystallites and this is a property typical of nanocrystalline materials [4]. The crystallite size of the synthesized nanoparticles of ZrO_2 can be estimated from the Debye-Scherrer equation. Broadening observed in the peaks indicated the presence of nanocrystalline zirconia as observed in FESEM where the particle size ranged between 46.35 to 65.66 nm, which is in good agreement with the observed peak broadening. More crystalline the XRD pattern, better the thermal stability, mechanical strength, catalytic activity, and chemical resistance it will exhibit, which is beneficial to applications. Diffraction patterns similar to this have been observed with nanocrystalline zirconia precipitates, hydrothermally synthesized, and synthesized by sol-gel processing [3,5] and it is considered that crystalline nanoparticles of zirconia had been successfully prepared.

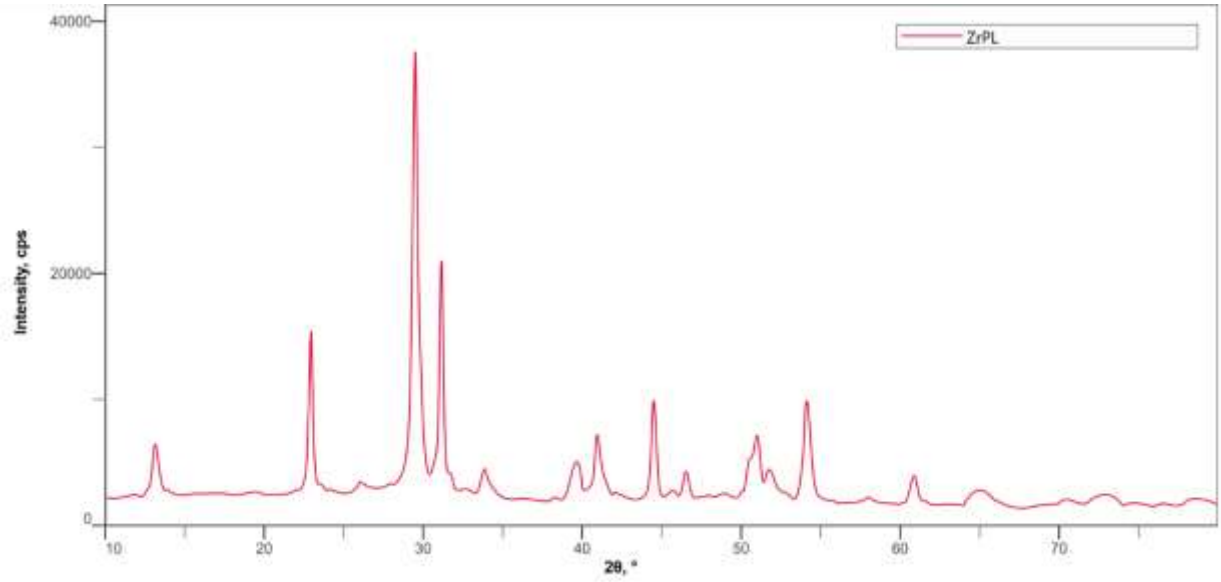

Figure 2: XRD analysis of Piper longum-mediated ZrO_2 nanoparticles

FESEM Analysis:

Field Emission Scanning Electron Microscopy was used to investigate the morphology and particle size distribution of ZrO_2 nanoparticles synthesized. Figure 3 is a FESEM micrograph taken at the following operating conditions: accelerating voltage, 15 kV; working distance, 9.7 mm; and magnification, 120,000×. The image shows the synthesized material on the nanoscale with a detailed view of its surface characteristics, covering a horizontal field width (HFW) of 3.45 µm. The FESEM image shows that synthesized particles (ZrO_2) have a spherical to nearly spherical shape with uniform distribution on the sample surface. The nanoparticles have a high tendency to agglomerate, i.e. they tend to form clusters of touching particles. This agglomeration is frequently seen for metal oxide nanoparticles because of the high surface energy of the nanoparticles, interparticle interactions during their synthesis and drying [1,2]. The analyzed FESEM micrograph gave a particle size of 46.35nm, 52.63nm, 56.21nm, 61.86nm and 65.66nm. The calculated average particle size is found to be about 56.54 nm, which confirms the synthesized zirconia to be of nanoscale size. The size distribution of particles is observed to be 46.35 nm to 65.66 nm, reflecting a relatively even particle development with slight particle size distribution. The width of the size range indicates that the synthesis process involves controlled nucleation and growth of the nanoparticles of ZrO_2 [3]. The surface morphology also illustrates the presence of a dense assembly of nanograins where the rough surface morphology is due to the aggregation of the particles. These nano-clusters may be explained by van der Waals attractive forces that occur between adjacent nanoparticles. Even so, the nanocrystalline particles still could be distinguished in the clusters, which means that the synthesis of independent nanosized zirconia particles was successfully achieved [4]. The particle size from FESEM is in concordance with what is expected for ZrO_2 materials in nanoscale and is like previously reported value of synthesized zirconia nanoparticles by precipitation process, sol-gel process, and hydrothermal method, where their particle size is in the range of 20-100 nm [2,5]. The small size of the particles is beneficial for the catalytic, sensing, adsorption and biomedical applications of zirconia nanomaterials [5]. In general, the FESEM investigation confirms successful preparation of nanostructured ZrO_2 having predominant spherical particles, average particles size 56.54 nm and moderately agglomerated morphology.

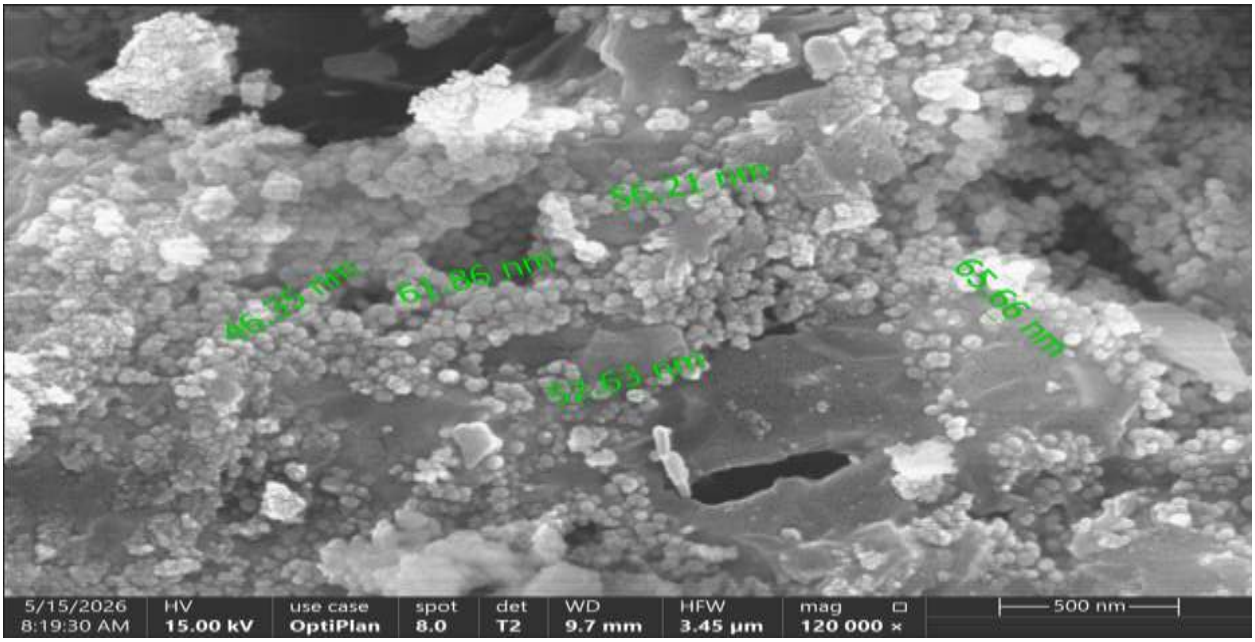

Figure 3: FESEM Analysis of Piper longum-mediated ZrO_2 nanoparticles

Raman Analysis:

Raman spectroscopy was performed to evaluate the vibrational characteristics, lattice features, and surface-associated molecular signatures of the Piper longum catkin extract-mediated zirconium oxide nanoparticles (Zr-PL / ZrO_2 NPs). The Raman spectrum showed distinct bands at approximately 123.84, 993.68, 1025.79, and 1063.72

cm^{-1} (Table 1 & Figure 4). The presence of a low-wavenumber band at 123.84 cm^{-1} indicates lattice-related vibration of the zirconium oxide framework. In ZrO_2 nanoparticles, Raman-active bands in the low-frequency region are generally associated with Zr–O lattice vibrations, phase-related phonon modes, and structural distortion within the oxide network. Therefore, the band observed at 123.84 cm^{-1} supports the formation of a zirconium oxide-based nanostructure. The bands observed at 993.68, 1025.79, and 1063.72 cm^{-1} are not typical primary lattice modes of pure zirconium oxide; rather, they may be attributed to surface-associated organic functional groups derived from the Piper longum catkin extract. These peaks can be associated with C–O, C–C, C–N, and C–O–C stretching vibrations of phytochemical residues present on the nanoparticle surface. Since Piper longum contains bioactive alkaloids and other oxygen- and nitrogen-containing phytoconstituents, the appearance of these high-wavenumber Raman bands suggests that plant-derived biomolecules remained attached to the surface of the ZrO_2 nanoparticles after synthesis. These biomolecules may have acted as natural capping and stabilizing agents during nanoparticle formation. The Raman profile also indicates that the synthesized nanoparticles possess both an inorganic zirconium oxide lattice and organic surface functionalization. The low-frequency band confirms the ZrO_2 vibrational contribution, while the higher-frequency bands reflect the presence of phytochemical residues from the plant extract. This is an important feature of green-synthesized nanoparticles because surface-bound biomolecules can influence particle stability, aggregation behavior, surface charge, and interaction with biological systems. In addition, surface defects, oxygen vacancies, and hydroxylated sites in ZrO_2 nanoparticles may contribute to reactive oxygen species generation and may therefore influence antimicrobial, antioxidant, and anticancer activities.

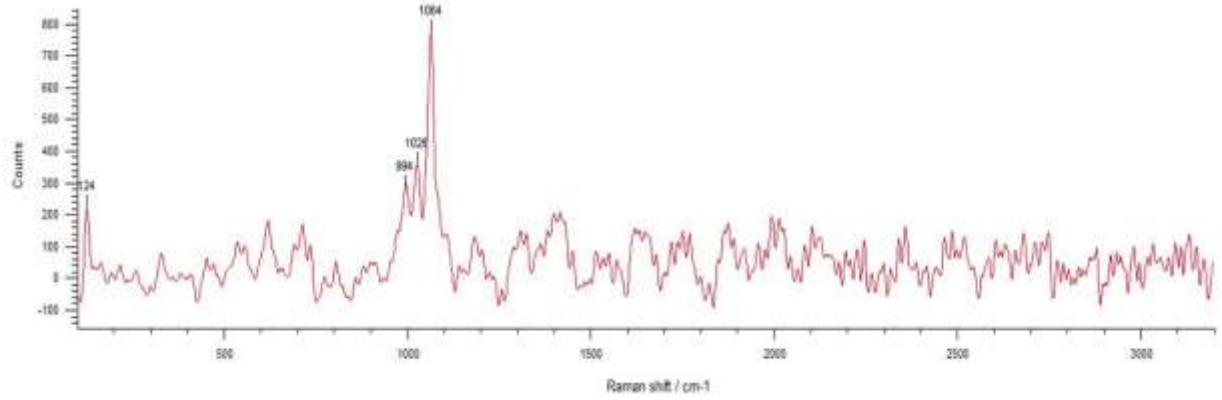

Figure 4: Raman Shift Analysis of Piper longum-mediated ZrO_2 nanoparticles

Table 1: Raman peak assignment of ZrO_2-PL nanoparticles

Raman band, cm^{-1}	Probable assignment	Interpretation
123.84	Zr–O lattice-related vibration / low-frequency phonon mode	Supports formation of zirconium oxide nanostructure
993.68	C–O / C–C / C–N stretching vibration	Surface-bound phytochemical residues from Piper longum
1025.79	C–O–C / C–N / organic stretching vibration	Indicates plant-derived capping molecules
1063.72	C–O stretching / organic functional group vibration	Confirms surface functionalization by extract-derived biomolecules

FTIR Analysis:

Fourier-transform infrared spectroscopy was performed to identify the functional groups involved in the formation and surface stabilization of the Piper longum extract-mediated zirconium oxide nanoparticles (ZrO_2 NPs/Zr-PL). The FTIR spectrum of Zr-PL showed absorption bands at 3833.79, 3745.08, 3428.81, 2487.72, 2140.60, 1770.33, 1673.91, 1646.91, 1461.78, 1153.22, 1049.09, 987.38, 871.67, 686.53, 605.54, and 478.26 cm^{-1} (Figure 5). These peaks indicate the presence of hydroxyl, carbonyl, C–O/C–N-containing phytochemical groups, and characteristic Zr–O

lattice vibrations, confirming the formation of phytochemically capped ZrO_2 nanoparticles. The absorption bands observed at 3833.79 and 3745.08 cm^{-1} may be assigned to free or weakly hydrogen-bonded O–H stretching vibrations, while the broad and intense band at 3428.81 cm^{-1} corresponds to O–H stretching of surface hydroxyl groups, adsorbed water molecules, and phenolic or alcoholic compounds derived from Piper longum extract. The presence of hydroxyl groups suggests that plant-derived biomolecules participated in the nucleation and stabilization of the nanoparticles. The weak bands at 2487.72 and 2140.60 cm^{-1} may be associated with adsorbed atmospheric species, weak organic residues, or surface-bound phytochemical components. The bands appearing at 1770.33, 1673.91, and 1646.91 cm^{-1} can be attributed to C=O stretching vibrations of carbonyl-containing compounds, C=C stretching vibrations, and/or H–O–H bending vibrations of adsorbed water. These peaks indicate the possible involvement of oxygen-containing phytoconstituents such as phenolics, alkaloids, flavonoid-like compounds, esters, or carboxyl-containing molecules in the green synthesis process. The strong absorption band at 1461.78 cm^{-1} may be assigned to C–H bending, C–N stretching, or carbonate-related vibrations. This band further supports the presence of organic residues from the Piper longum extract on the nanoparticle surface. The bands in the fingerprint region at 1153.22, 1049.09, and 987.38 cm^{-1} are mainly associated with C–O, C–N, and C–O–C stretching vibrations of plant-derived biomolecules. These functional groups may coordinate with zirconium ions during synthesis and act as natural stabilizing or capping agents. The absorption band at 871.67 cm^{-1} may be related to out-of-plane C–H bending or Zr–O–C type surface interactions, suggesting bonding or adsorption between phytochemical residues and the zirconium oxide surface. The low-wavenumber bands at 686.53, 605.54, and 478.26 cm^{-1} are the most important indicators for zirconium oxide formation. These bands are attributed to Zr–O and Zr–O–Zr stretching vibrations, confirming the development of the zirconium oxide framework. The appearance of these metal–oxygen bands, together with organic functional group signals, demonstrates that the synthesized nanoparticles consist of an inorganic ZrO_2 core capped or stabilized by bioactive compounds from Piper longum extract.

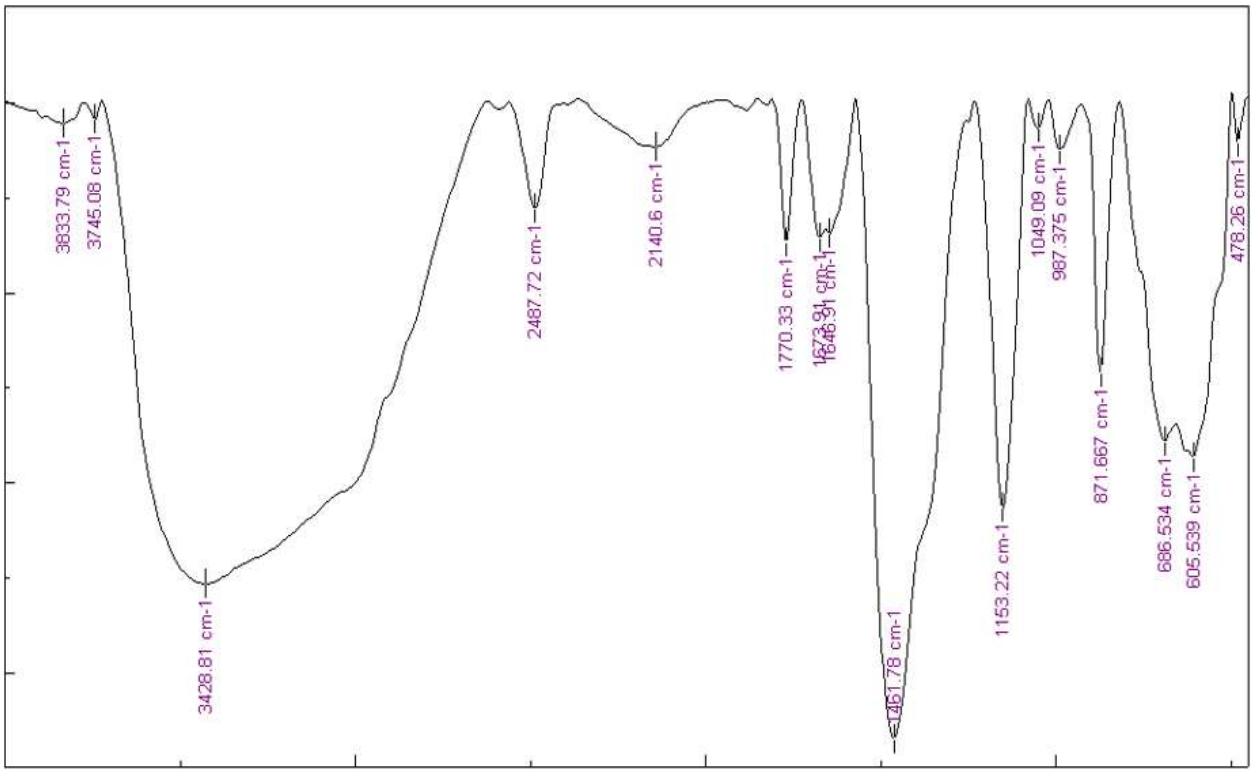

Figure 5: FTIR Analysis of Piper longum-mediated ZrO_2 nanoparticles

EDS Analysis:

The elemental composition of the synthesized nanoparticles of zirconium oxide (ZrO_2) was determined by the Energy Dispersive X-ray Spectroscopy (EDS) and the result is presented in the spectrum and quantitative result (shown in figure 6 & Table 2). The EDS was taken at 15-kV accelerating voltage and a total acquisition time of 55 s. A total of 213,499 counts were obtained and the average count rate was 3,899 cps ensuring a good level of reliability for elemental identification and quantitative analysis. Only two peaks associated with oxygen (O) and zirconium (Zr) can be seen in the EDS spectrum. The oxygen peak is due to the O-K emission line, and the zirconium peak is due to the Zr-L emission line. No other metal or metal oxide peaks could be observed within the detection limits of the instrument, which confirms the high elemental purity of the synthesized nanoparticles, and suggests that there was no significant contamination of the nanoparticles during the synthesis steps [1,2]. The results of quantitative elemental analysis showed that oxygen is 70.2 at% and 29.2 wt% while zirconium is 29.8 at% and 70.8 wt%. The net counts are 13,449 for oxygen and 68,288 for zirconium, with very strong characteristic X-ray signals from both the constituent elements. There was high confidence in the quantitative measurements as the corresponding analytical uncertainties were relatively low, with atomic percentage errors for oxygen (0.7%) and zirconium (0.2%) and weight percentage errors for oxygen (0.3%) and zirconium (0.5%). The composition of the obtained atoms is in close agreement with the theoretical composition of zirconium oxide, ZrO_2, that is, the ratio of oxygen atoms to zirconium atoms is two to one [3]. Minor deviations from the ideal stoichiometry are generally found in EDS measurements arising from surface morphology, particle agglomeration, detector sensitivity and the relatively low X-ray generation efficiency of light elements like oxygen; however, the measured composition exhibits consistency with the formation of zirconia nanoparticles [4]. In addition, the high peaks of zirconium and oxygen and the lack of other elemental peaks indicate that the material produced may be largely zirconium oxide. The results of the EDS thus confirm the successful synthesis of ZrO_2 nanoparticles and indicate the chemical purity of the sample. The elemental distribution and the typical EDS spectra of ZrO2 have been reported for hydrothermal and precipitation-based synthesis of pure ZrO2 nanoparticles [4,5].

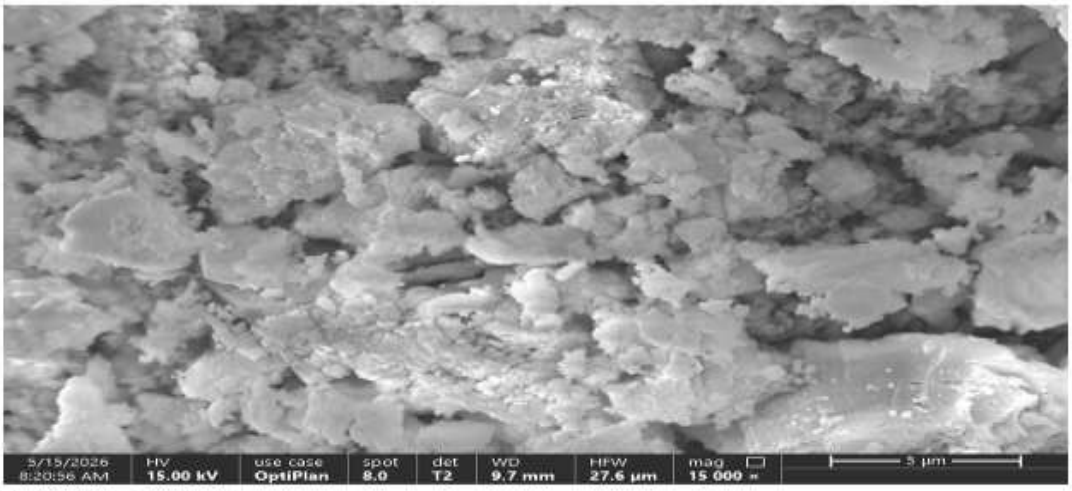

Total Number of Counts: 213 499
Average Count Rate: 3 899 cps
Acceleration Voltage: 15 kV
Total Acquisition Time: 55 seconds

Element	Line	At. %	Wt. %	Net Counts	At. % Error	Wt. % Error
O	K	70.2	29.2	13 449	0.7	0.3
Zr	L	29.8	70.8	68 288	0.2	0.5

Figure 6: EDS Analysis of Piper longum-mediated ZrO_2 nanoparticles

Table 2: Major FTIR Band details of Piper longum-mediated ZrO_2 nanoparticles

Sample	Major FTIR bands, cm^{-1}	Probable assignment
Zr-Pl	3833.79, 3745.08, 3428.81	O–H stretching of hydroxyl groups and adsorbed water
Zr-Pl	1770.33, 1673.91, 1646.91	C=O stretching / H–O–H bending / organic phytochemical residues
Zr-Pl	1461.78	C–H bending, C–N stretching, or carbonate-related vibration
Zr-Pl	1153.22, 1049.09	C–O / C–N stretching of biomolecules

Antimicrobial Activity:

The newly synthesized Zr-PL nanoparticles (Piper longum-mediated ZrO_2 NPs) were screened for antimicrobial activities by the agar well diffusion method against four bacteria (S. aureus, E. coli, B. subtilis and P. aeruginosa) and fungal strain (C. albicans). Three concentrations (5, 10 and 25 mg mL-1) were tested for their antibacterial activity and the results were compared with standard antibiotic streptomycin (1 mg mL-1) and the standard antifungal agent fluconazole (1 mg mL-1). The results showed that the antimicrobial effect of Zr-PL nanoparticles was concentration-dependent, as their concentration increased, the inhibitory effect against the tested microorganisms increased. The zone of inhibition for Staphylococcus aureus was 1 mm at 5 mg mL-1, 2 mm at 10 mg mL-1 and 3 mm at 25 mg mL-1. A similar pattern was seen for Escherichia coli with inhibition zones of 1mm, 2mm and 3mm at 5mg mL-1, 10mg mL-1 and 25mg mL-1 respectively. The inhibition zones obtained were 1 mm, 2 mm and 4 mm at concentration of 5 mg mL-1, 10 mg mL-1 and 25 mg mL-1 respectively against Bacillus subtilis. The zone of inhibition was maximum with Zr-PL nanoparticles against Pseudomonas aeruginosa among the tested bacterial strains with the zone size increasing from 1mm at 5mg/mL to 2mm at 10mg/mL up to 5mm at 25mg/mL. Though these values were quite lower than that of the standard antibiotics streptomycin which has produced inhibition zones of 35, 32, 30 and 33 mm against S. aureus, E. coli, B. subtilis and P. aeruginosa, respectively, the result has proved the intrinsic antibacterial activity of synthesized Zr-PL nanoparticles [1,2]. Concentration-dependent responses also observed in the antifungal activity against Candida albicans. The diameters of inhibition zones were observed to be 1 mm, 2 mm and 3 mm at concentrations of 5 mg mL-1, 10 mg mL-1 and 25 mg mL-1, respectively. The antifungal activity was significantly high, with the standard antifungal drug fluconazole showing a larger inhibition zone of 35 mm in comparison. However, the inhibition effect shown by the Zr-PL nanoparticles indicates that the nanoparticles can inhibit the growth of fungi to some extent [3]. The antimicrobial activity of Zr nanoparticles might be due to the large surface area, direct attack on the microbial cell wall, production of reactive oxygen species (ROS), and damage to critical cellular functions. All these processes can result in damage of the membranes, membrane permeability, oxidative stress and ultimately loss of microbial life [2,4]. The increased inhibition at higher concentrations may be supported by the greater number of active nanoparticles to interact with microbial cells. In general, the synthesized Zr-PL nanoparticles appeared to have measurable antibacterial and antifungal activities with the highest activity noted at 25 mg mL-1.

Microorganism / Sample	Piper longum mediated Mn-NPs
E. coli	
Staphylococcus aureus	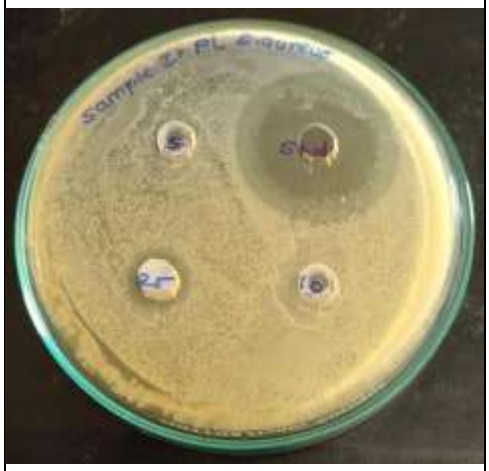
Bacillus subtilis	

Pseudomonas aeruginosa	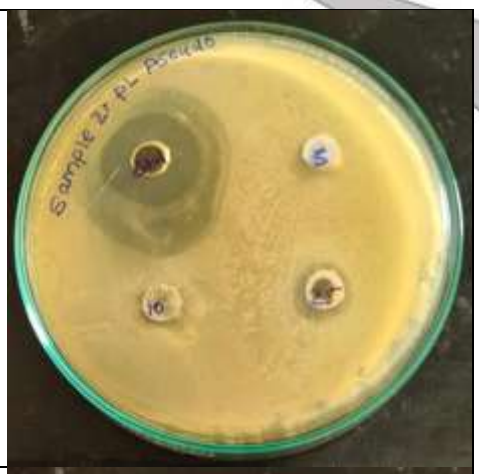
Candida albicans	

Figure 7: Antimicrobial Activity of Piper longum-mediated ZrO_2 nanoparticles

Table 3: Zone of Inhibition of Piper longum-mediated ZrO_2 NPs for various concentrations

Sr. No.	Sample	Concentration (mg/ml)	Zone of Inhibition (mm)				
			S. aureus	E. coli	B. subtilis	P. aeruginosa	C. albicans
1	Control	-	-	-	-	-	-
2	Standard Streptomycin	1	35	32	30	33	35
3	Sample Piper longum-ZrO_2 NPs	5	01	01	01	01	01
		10	02	02	02	02	02
		25	03	03	04	05	03

Antioxidant Activity:

The antioxidant activity of the synthesized Zr-PL nanoparticles was evaluated using the DPPH free radical scavenging assay at concentrations ranging from 200 to 1000 µg/mL (Figure 8 & Table 4). The results showed a gradual increase in DPPH radical scavenging activity with increasing nanoparticle concentration, indicating a concentration-dependent antioxidant response. At 200 µg/mL, Zr-PL nanoparticles exhibited 36.77% inhibition, which increased to 37.91% at 400 µg/mL. Further enhancement in antioxidant activity was observed at 600 µg/mL and 800 µg/mL, with inhibition values of 41.06% and 41.93%, respectively. The highest scavenging activity was recorded at 1000 µg/mL, where Zr-PL nanoparticles showed 43.64% inhibition. The mean absorbance decreased from 0.776 at 200 µg/mL to 0.692 at 1000 µg/mL, confirming the ability of Zr-PL nanoparticles to reduce DPPH radicals. This reduction in absorbance reflects the conversion of the purple DPPH radical into its reduced form, indicating free radical

scavenging potential. The antioxidant behavior of Zr-PL nanoparticles may be associated with the combined effect of zirconium oxide surface activity and phytochemical residues derived from Piper longum extract. During green synthesis, plant-derived functional groups can remain adsorbed on the nanoparticle surface and act as natural capping agents. These surface-bound biomolecules may contribute to radical neutralization through electron transfer or hydrogen donation.

Although the antioxidant activity increased with concentration, the maximum inhibition observed was 43.64% at 1000 µg/mL. Since the scavenging activity did not reach 50% within the tested concentration range, the IC_{50} value may be considered greater than 1000 µg/mL under the present experimental conditions. This suggests that Zr-PL nanoparticles possess moderate antioxidant activity, with improved radical scavenging efficiency at higher concentrations. The antioxidant potential of green-synthesized zirconium oxide nanoparticles has been reported in previous studies, where plant-mediated ZrO_2 nanoparticles demonstrated DPPH radical scavenging activity due to surface-bound phytochemicals and oxide nanoparticle surface interactions. Therefore, the observed antioxidant activity of Zr-PL nanoparticles may be attributed to the phytochemical capping effect of Piper longum extract along with the surface properties of zirconium oxide nanoparticles.

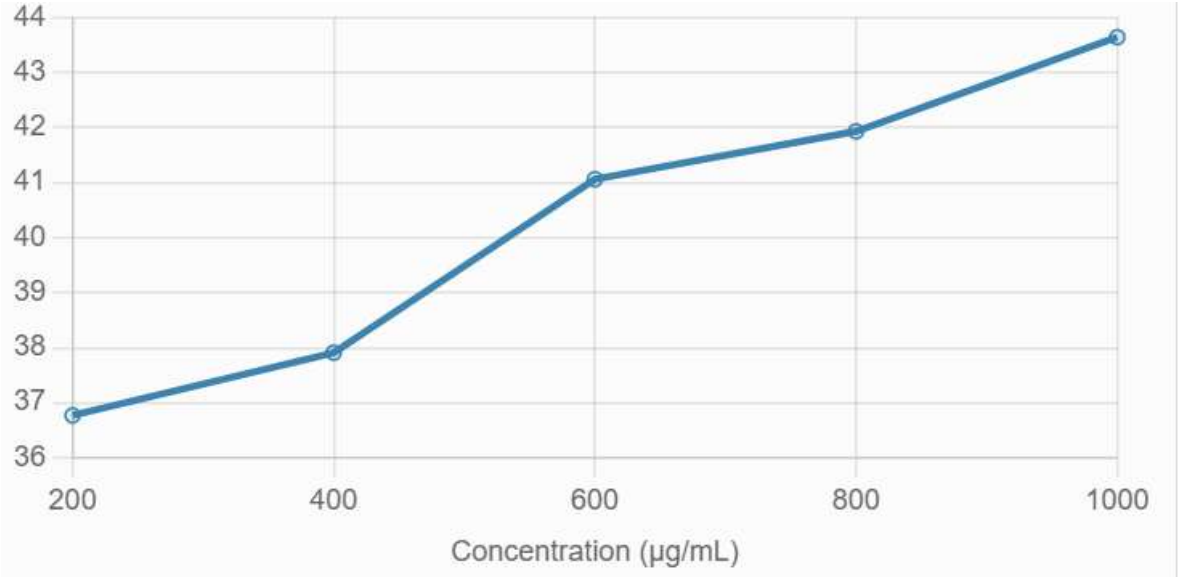

Figure 8: Antioxidant Activity of Piper longum-mediated ZrO_2 nanoparticles

Table 4: DPPH radical scavenging activity of Zr-PL nanoparticles

Sample	Concentration /mL	Abs 1	Abs 2	Abs 3	Mean Abs	Inhibition %
Zr-PL	200	0.776	0.778	0.774	0.776	36.77
	400	0.754	0.768	0.764	0.762	37.91
	600	0.725	0.724	0.721	0.723	41.06
	800	0.712	0.714	0.712	0.713	41.93
	1000	0.698	0.699	0.678	0.692	43.64

Anticancer Activity:

The in vitro anticancer activity of the synthesized Zr-PL nano-particles was evaluated against human lung adenocarcinoma (A549) and cervical adenocarcinoma (HeLa) cell lines and the results obtained showed that the synthesized Zr-PL nano-particles showed significant concentration-dependent, anticancer activity. In the A549 cell line, untreated control cells exhibited an average absorbance value of 2.110 ± 0.002, indicating maximum cell viability, whereas treatment with Zr-PL nanoparticles progressively reduced the absorbance values to 1.403 ± 0.0015, 1.304 ± 0.0021, 1.223 ± 0.0020, 0.944 ± 0.0028, and 0.834 ± 0.0021 at concentrations of 6.25, 12.5, 25, 50, and 100

μg mL^{-1}, respectively. The percentage cell viability was therefore reduced with the increasing concentration of the nanoparticles, that is, from 66.50% at 6.25 μg mL^{-1}, 61.81%, 57.95%, 44.75% and 39.54%, respectively, showing the good inhibition of cell proliferation. The IC_{50} of the Zr-PL nanoparticles at A549 cell line was measured as 53.18 μg mL-1 that revealed the potent cytotoxic effect of the nanoparticles against lung cancer cells. A comparable trend was observed in the HeLa cell line, where the untreated control exhibited an average absorbance value of 2.324 ± 0.0032, while exposure to Zr-PL nanoparticles reduced the absorbance values to 1.454 ± 0.0038, 1.356 ± 0.0036, 1.346 ± 0.1585, 1.114 ± 0.0021, and 0.944 ± 0.0021 at concentrations of 6.25, 12.5, 25, 50, and 100 μg mL^{-1}, respectively. The five cell viability measurable values were 62.58%, 58.33%, 57.90%, 47.94%, and 40.62%, which indicated a strong inhibitory effect on the growth of cervical cancer cells. The calculated IC50 value for HeLa cell was 53.93 μg mL-1 that was very close to that of A549 cell which indicates that the Zr-PL nanoparticles display almost similar cytotoxic activity towards both the cancer cell types. IC_{50} values were calculated by comparing with the standard chemotherapeutic agent 5-fluorouracil (5-FU), with values of 14.55 and 34.71 μg mL^{-1} for the HeLa and A549 cells respectively, showing that the synthesized Zr-PL nanoparticles had respectable cytotoxic activity for the cells tested while the standard drug was more potent against the cancer cells. Interestingly, the highest tested concentration of Zr-PL nanoparticles (100 μg mL^{-1}) caused only about 60% growth inhibition in A549 cells and 40.62% growth inhibition in HeLa cells, respectively. Observed decrease in cell viability as a function of increasing concentration indicates the efficient interaction of the nanoparticles with cancer cells and suppression of metabolic activity and cancer cell proliferation. It has been suggested that the anticancer activity of zirconia-based nanomaterials is related to their small size, high surface-to-volume ratio, increased cellular uptake, production of reactive oxygen species (ROS), induction of oxidative stress, disruption of mitochondrial membranes, binding to and/or damage of DNA, and triggering of apoptotic-related signaling pathways [1,2]. In general, the MTT assay result showed that Zr-PL nanoparticles showed strong anticancer activity toward both cancer cell lines (A549 and HeLa), with slightly higher activity towards A549 cell, as presented by the lower IC50 value. The results show that Zr-PL nanoparticles could be considered as a potential nanomaterial for the treatment of cancer, and additional studies will be needed to better understand their mechanism of action and to test their efficacy in vivo.

Sr. No.	**Cell Line**	**Sample**	**Concentration (μg/ml)**	**Absorbance (OD)**				**Cell Viability (%)**	**IC_{50} (μg/ml)**
				1	**2**	**3**	**Average**		
1	-	Control	-	2.321	2.326	2.327	2.324±0.003215	-	-
2	-	5FU – HeLa	6.25	1.325	1.326	1.329	1.326±0.002082	57.08	**14.55**
			12.5	0.811	0.815	0.816	0.814±0.002646	35.02	
			25	0.741	0.745	0.743	0.743±0.002	31.97	
			50	0.514	0.515	0.516	0.515±0.001	22.16	
			100	0.412	0.415	0.416	0.414±0.0902082	17.82	
3	-	5FU – A549	6.25	1.625	1.623	1.629	1.625±0.003055	77.04	**34.71**
			12.5	1.524	1.523	1.526	1.524±0.001528	72.24	
			25	1.421	1.42	1.423	1.421±0.001528	67.36	
			50	0.954	0.952	0.956	0.954±0.002	42.51	
			100	0.841	0.842	0.846	0.843±0.002646	39.95	
3	A549	Sample Piper longum-Mn NPs	6.25	1.402	1.405	1.403	1.403±0.001528	66.50	**53.18**
			12.5	1.302	1.305	1.306	1.304±0.002082	61.81	
			25	1.221	1.225	1.223	1.223±0.002	57.95	
			50	0.942	0.945	0.946	0.944±0.002082	57.49	
			100	0.835	0.832	0.836	0.834±0.002082	39.54	
4	HeLa		6.25	1.452	1.453	1.459	1.454±0.003786	62.58	**53.92**
			12.5	1.352	1.359	1.357	1.356±0.003606	58.33	
			25	1.256	1.253	1.529	1.346±0.15849	57.90	
			50	1.115	1.112	1.116	1.114±0.002082	47.94	
			100	0.942	0.945	0.946	0.944±0.002082	40.62231	

Table 5: Effects of Piper longum-mediated ZrO_2 against 5-FU, A549, and HeLa cell lines by MTT Assay

(a)

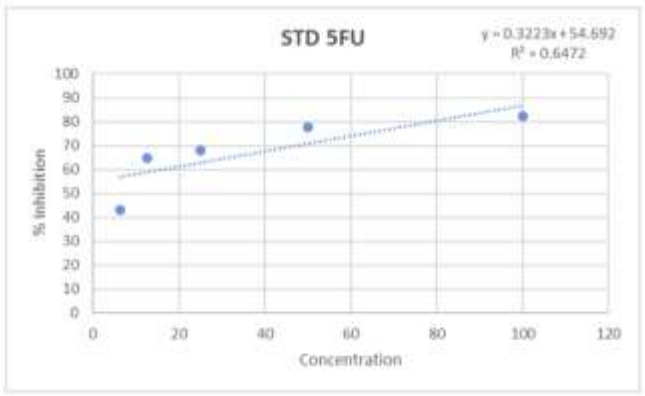

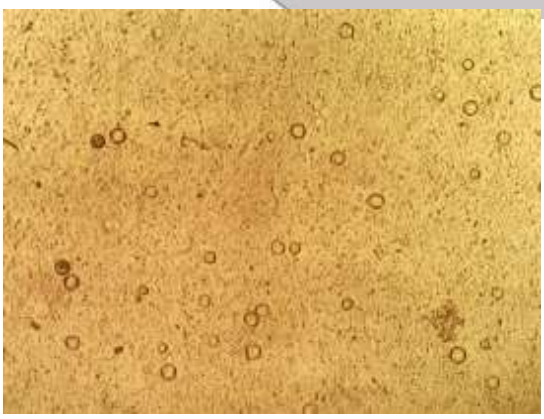

(b)

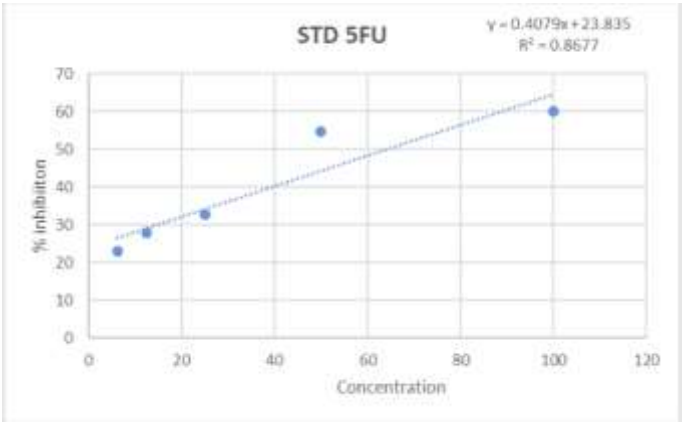

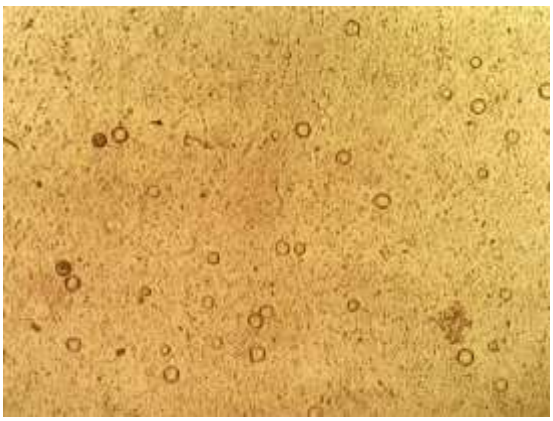

(c)

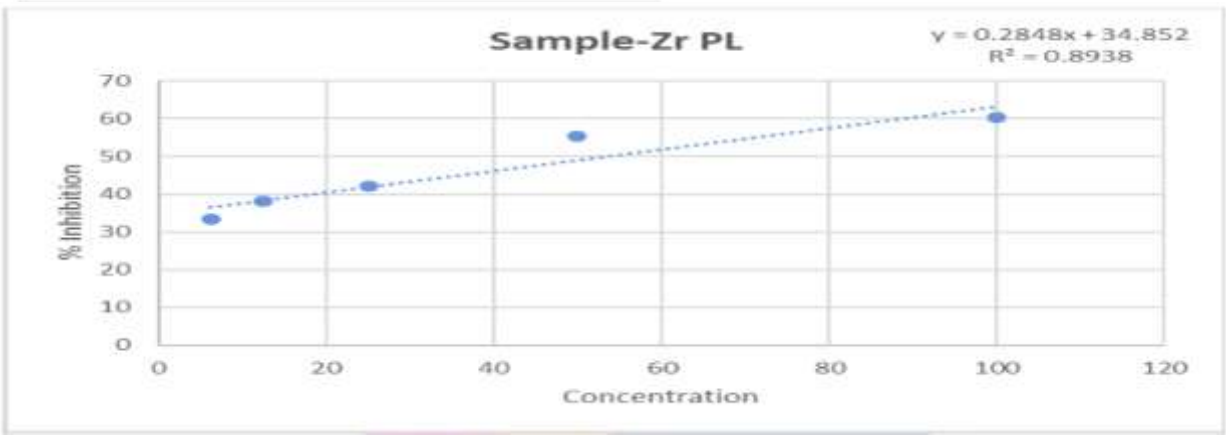

(d)

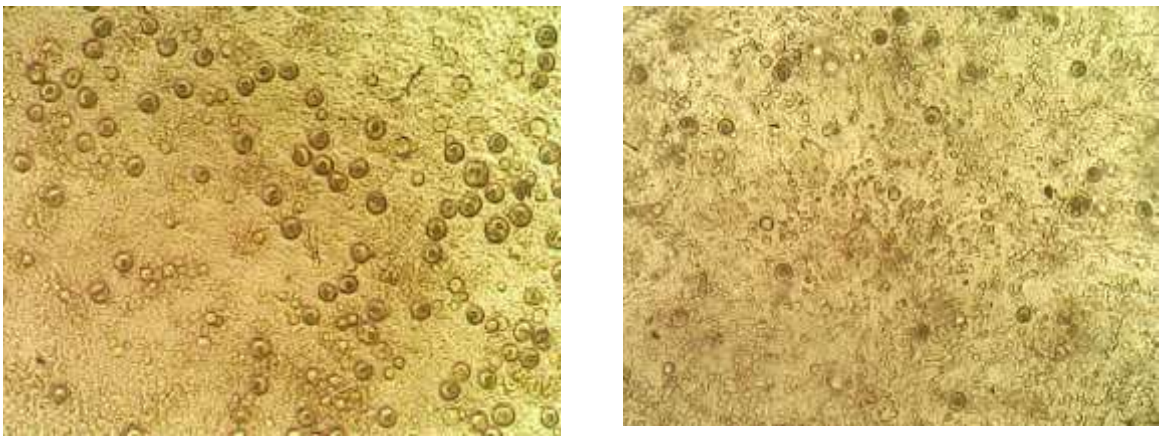

Figure 9: Anticancer activity of Piper longum-mediated ZrO_2 NPs against (a) 5-FU (A549), (b) 5-FU (HeLa), A549, and (c) HeLa

Conclusion & Future Perspectives:

Utilization of Piper longum catkin extract in the green synthesis of zirconium oxide (ZrO_2) nanoparticles was successfully achieved and highlighted as a sustainable and eco-friendly biogenic approach. As per structural characterization by XRD highly crystalline and phase pure Zro2 nanoparticles were observed and FESEM analysis showed predominantly spherical nature of the nanoparticles with an average particle size of 56.54 nm. The elemental purity from EDS analysis of the synthesized material was done by the presence of only the elements zirconium and oxygen. Raman and FTIR studies also confirmed the formation of the ZrO_2 framework and illustrated the involvement of various natural phyto-chemicals of Piper longum as natural reducing, capping and stabilizing agents. The utilization of the biomolecules of plants on the surface of the nanoparticle demonstrates the effectiveness of green synthesis technique in preparing stable and functionalized nanomaterials.

Biological evaluation showed that the prepared Zr-PL nanoparticles had concentration-dependent antimicrobial, antioxidant and anticancer properties. The nanoparticles exhibited antimicrobial activity against Gram-negative (G-) bacteria, Gram-positive (G+) bacteria and Candida albicans with the highest activity against Pseudomonas aeruginosa at 25 mg mL-1. The DPPH radical scavenging assay showed moderate antioxidant activity with the maximum inhibition of 43.64% at 1000 µg mL^{-1}. Moreover, MTT assay showed that this polymer has a significant cytotoxic effect against A549 and HeLa cancer cells with IC_{50} values 53.18 and 53.93 µg mL^{-1}, respectively. The biological activity of Zr-PL nanoparticles is hypothesized to be a synergistic effect of the nanoscale size of nanoparticles, their high surface area, reactivity of zirconia surface, and bioactive phytochemicals functionalized on the surface of nanoparticles.

Although remarkable achievements have been accomplished in the eco-friendly synthesis of metal oxide nanoparticles, the use of Piper longum catkin extract for the synthesis of ZrO_2 nanoparticles has been limited to few studies and systematic correlation of its physico-chemical properties with its multifunctional bioactivities has not been investigated. In the present work, it aims to explore this area and offer a thorough investigation into the structural, morphological, compositional, antimicrobial, antioxidant and anticancer properties of the Piper longum mediated Zirconia nanoparticles. Unfortunately, the exact mechanisms underlying their biological activity are not well understood. In particular, the involvement of surface phytochemicals, the generation of reactive oxygen species, transport mechanisms by cells, and the signaling pathways involved in apoptosis remain further to be elucidated.

More detailed mechanistic investigations, including ROS generation, mitochondrial dysfunction, gene expression profiling, and cell-cycle arrest analysis, as well as studying the changes of apoptosis pathways should be encouraged in future studies to elucidate the anti-cancer actions of Zr-PL nanoparticles. Furthermore, in vivo toxicity, pharmacokinetic, biodistribution and therapeutic efficacy studies are required prior to any clinical or biomedical

applications. Their therapeutic potential may be further enhanced by surface modification, drug-loading capacity, targeted delivery approaches, and optimization of formulation of nanoparticles. Furthermore, the idea of extending to other microbial pathogens and cancer cell lines could yield a greater understanding of their wide biomedical applications. In summary, the results of this study make ZrO_2 nanoparticles synthesized using Piper longum SEED powder as the reducing agent as prospective multi-functional nanomaterials and give a solid ground to the creation of sustainable nanotechnology based therapeutic and biomedical applications with environmental years.

References:

[1] Unni, V., Abishad, P., Prasastha Ram, V., Niveditha, P., Yasur, J., John, L., … Rawool, D. B. (2024). Green synthesis, and characterization of zinc oxide nanoparticles using Piper longum catkin extract and its in vitro antimicrobial activity against multi-drug-resistant non-typhoidal Salmonella spp. Inorganic and Nano-Metal Chemistry, 54(9), 849–857. https://doi.org/10.1080/24701556.2022.2078356

[2] Daphne Mary Johna, Nilesh S, Pillaia, Akshay Sivana, Lasya P Archana P, K.M. Sreekanth, Sivasubramanian, Sreedhar K.M, "Ferromagnetic $_{ZrO2}$ nanostructures from an organo zinc complex formulated via Piper longum L-assisted green synthesis: Multifaceted prospects in photocatalysis, antimicrobial activity, and cell viability studies", Research article Volume 10, Issue 13e33360July 15, 2024Open access https://www.cell.com/heliyon/fulltext/S2405-8440(24)09391-5

[3] Asha S, Bessy TC, Joe Sherin JF, Vani CV, Kumar CV, Bindhu MR, Sureshkumar S, Al-Khattaf FS, Hatamleh AA. Efficient photocatalytic degradation of industrial contaminants by Piper longum mediated $_{ZrO2}$ nanoparticles. Environ Res. 2022 May 15;208:112686. doi: 10.1016/j.envres.2022.112686. https://pubmed.ncbi.nlm.nih.gov/35032540/

[4] Tran XT, Bien TTL, Tran TV, Nguyen TTT. Biosynthesis of $_{ZrO2}$ nanoparticles using aqueous extracts of Eclipta prostrata and Piper longum: characterization and assessment of their antioxidant, antibacterial, and photocatalytic properties. Nanoscale Adv. 2024 Aug 7;6(19):4885-4899. doi: 10.1039/d4na00326h. https://pubmed.ncbi.nlm.nih.gov/39323417/

[5] Vas NV, Sundari SK, Jeyachandran S. Degradation of Microplastics by Zinc Oxide Nanoparticles Synthesized Using Piper longum Leaf Extract. Cureus. 2024 Sep 21;16(9):e69876. doi: 10.7759/cureus.69876. https://pubmed.ncbi.nlm.nih.gov/39439655/

[6] Rao SP, Byrappa K, Keerthiraj N, Chatterjee J, Mustak MS. Phyto-Fabrication of $_{ZrO2}$ Nanoparticles Using Piper betel Aqueous Extract and Evaluation of its Applicability in Dentistry. Pharm Nanotechnol. 2018;6(3):201-208. doi: 10.2174/2211738506666180611101852. https://pubmed.ncbi.nlm.nih.gov/29886841/

[7] Truong TT, Khieu TT, Luu HN, Truong HB, Nguyen VK, Vuong TX, Tran TKN. Characterization and Bioactivity of Piper chaudocanum L. Extract-Doped $_{ZrO2}$ Nanoparticles Biosynthesized by Co-Precipitation Method. Materials (Basel). 2023 Aug 3;16(15):5457. doi: 10.3390/ma16155457. https://pubmed.ncbi.nlm.nih.gov/37570161/

[8] Sohrabi S, Kargar M, Ramezani A, Moazamian E, Ebrahiminezhad A, Berenjian A. Phytochemical-Mediated Synthesis of Zinc Oxide Nanoparticles with Enhanced Antimicrobial Properties. Mol Biotechnol. 2026 May;68(5):2486-2496. doi: 10.1007/s12033-025-01515-4. https://pubmed.ncbi.nlm.nih.gov/41076492/

[9] Kumar A, Shrivastava A, Suttee A, Gupta P, Shahi S, Barik R, Chaturvedi P, Dwivedi S. Plant-Powered Nanotechnology: A Review of Green Synthesis Approaches for $_{ZrO2}$ and Silver Nanoparticles with Medicinal Flora. Curr Top Med Chem. 2026 Jan 16. doi: 10.2174/0115680266413831251120132852. https://pubmed.ncbi.nlm.nih.gov/41582585/

[10] Mobinhosseini F, Salehirad M, Wallace Hayes A, Motaghinejad M, Hekmati M, Safari S, Gholami M. Curcumin-$_{ZrO2}$ conjugated nanoparticles confer neuroprotection against ketamine-induced neurotoxicity. J Biochem Mol Toxicol. 2024 Jan;38(1):e23611. doi: 10.1002/jbt.23611. https://pubmed.ncbi.nlm.nih.gov/38084605/

[11] Girardello F, Leite CC, Touguinha LB, Roesch-Ely M, da Silva CKH, de Oliveira RM, Borges DLG, Villela IV, Fernandes AN, Salvador M, Henriques JAP. $_{ZrO2}$ nanoparticles alter redox metabolism of Limnoperna fortunei. Environ Sci Pollut Res Int. 2021 Dec;28(48):69416-69425. doi: 10.1007/s11356-021-15257-8. https://pubmed.ncbi.nlm.nih.gov/34302239/

[12] Subramaniam VD, Prasad SV, Banerjee A, Gopinath M, Murugesan R, Marotta F, Sun XF, Pathak S. Health hazards of nanoparticles: understanding the toxicity mechanism of nanosized $_{ZrO2}$ in cosmetic products. Drug Chem Toxicol. 2019 Jan;42(1):84-93. doi: 10.1080/01480545.2018.1491987. https://pubmed.ncbi.nlm.nih.gov/30103634/

[13] Udayagiri H, Sana SS, Dogiparthi LK, Vadde R, Varma RS, Koduru JR, Ghodake GS, Somala AR, Boya VKN, Kim SC, Karri RR. Phytochemical fabrication of $_{ZrO2}$ nanoparticles and their antibacterial and anti-biofilm activity. Sci Rep. 2024 Aug 24;14(1):19714. doi: 10.1038/s41598-024-69044-9. https://pubmed.ncbi.nlm.nih.gov/39181904/
[14] Ahmed T, Ren H, Noman M, Shahid M, Liu M, Ali MA, Zhang J, Tian Y, Qi X, Li B. Green synthesis and characterization of zirconium oxide nanoparticles by using a native Enterobacter sp. and its antifungal activity against bayberry twig blight disease pathogen Pestalotiopsis versicolor. NanoImpact. 2021 Jan;21:100281. doi: 10.1016/j.impact.2020.100281. https://pubmed.ncbi.nlm.nih.gov/35559773/
[15] Pradeep L, Thangavelu I, Suriyaprakash J, Arulselvan P, Salmen SH, Chinnathambi A, Boopathi TS. Bougainvillea glabra-mediated synthesis of Zr_3O and chitosan-coated zirconium oxide nanoparticles: Multifunctional antibacterial and anticancer agents with enhanced biocompatibility. Int J Biol Macromol. 2025 Apr;300:139609. doi: 10.1016/j.ijbiomac.2025.139609. https://pubmed.ncbi.nlm.nih.gov/39809398/
[16] Rozina, Ahmad M, Zafar M. Conversion of waste seed oil of Citrus aurantium into methyl ester via green and recyclable nanoparticles of zirconium oxide in the context of circular bioeconomy approach. Waste Manag. 2021 Dec;136:310-320. doi: 10.1016/j.wasman.2021.10.001. https://pubmed.ncbi.nlm.nih.gov/34749274/
[17] Sadiq MU, Shah A, Haleem A, Shah SM, Shah I. Eucalyptus globulus Mediated Green Synthesis of Environmentally Benign Metal Based Nanostructures: A Review. Nanomaterials (Basel). 2023 Jul 6;13(13):2019. doi: 10.3390/nano13132019. https://pubmed.ncbi.nlm.nih.gov/37446535/
[18] Kathirvel A, Srinivasan R, Sasikumar M, Ranjith N, Srinivasan R, Karthika R, Atchudan R, Natarajan D, Wadaan MA, Srinivasan P, Yun HK. Green Synthesis of ZrO_2 Nanoparticles From Gardenia resinifera for Efficient Photocatalytic Methylene Blue Dye Degradation With Antimicrobial and Antioxidant Properties. Luminescence. 2025 Jun;40(6):e70223. doi: 10.1002/bio.70223. https://pubmed.ncbi.nlm.nih.gov/40506268/
[19] Sharma S, Bharti R, Sharma R. Green Synthesis of ZrO_2 Nanoparticles from Cynodon dactylon: Structural Characterization, Antioxidant Performance, and Corrosion Inhibition of Mild Steel. Chempluschem. 2026 Apr;91(4):e202600006. doi: 10.1002/cplu.202600006. https://pubmed.ncbi.nlm.nih.gov/41936544/
[20] Shanmuganathan R, LewisOscar F, Shanmugam S, Thajuddin N, Alharbi SA, Alharbi NS, Brindhadevi K, Pugazhendhi A. Core/shell nanoparticles: Synthesis, investigation of antimicrobial potential and photocatalytic degradation of Rhodamine B. J Photochem Photobiol B. 2020 Jan;202:111729. doi: 10.1016/j.jphotobiol.2019.111729. https://pubmed.ncbi.nlm.nih.gov/31835161/
[21] Rana R, Ahmad W, Mishra A, Kumar S, Ahmed S, Ansari SA. Efficient Photocatalytic Degradation of Dyes Under Natural Solar Light Using Facile One-Step Green Synthesized ZrO_2 Nanoparticles. Microsc Res Tech. 2025 Sep;88(9):2528-2544. doi: 10.1002/jemt.24870. https://pubmed.ncbi.nlm.nih.gov/40245357/
[22] Debnath B, Majumdar M, Bhowmik M, Bhowmik KL, Debnath A, Roy DN. The effective adsorption of tetracycline onto zirconia nanoparticles synthesized by novel microbial green technology. J Environ Manage. 2020 May 1;261:110235. doi: 10.1016/j.jenvman.2020.110235. https://pubmed.ncbi.nlm.nih.gov/32148305/
[23] Shahamirifard SA, Ghaedi M, Razmi Z, Hajati S. A simple ultrasensitive electrochemical sensor for simultaneous determination of gallic acid and uric acid in human urine and fruit juices based on zirconia-choline chloride-gold nanoparticles-modified carbon paste electrode. Biosens Bioelectron. 2018 Aug 30;114:30-36. doi: 10.1016/j.bios.2018.05.009. https://pubmed.ncbi.nlm.nih.gov/29775856/
[24] Gao N, He C, Ma M, Cai Z, Zhou Y, Chang G, Wang X, He Y. Electrochemical co-deposition synthesis of Au-ZrO2-graphene nanocomposite for a nonenzymatic methyl parathion sensor. Anal Chim Acta. 2019 Sep 23;1072:25-34. doi: 10.1016/j.aca.2019.04.043. https://pubmed.ncbi.nlm.nih.gov/31146862/
[25] Lotfi L, Javadpour J, Naimi-Jamal MR. Biological and nano-indentation properties of polybenzoxazine-based composites reinforced with zirconia particles as a novel biomaterial. Biomed Mater Eng. 2018;29(3):369-387. doi: 10.3233/BME-181731. https://pubmed.ncbi.nlm.nih.gov/29578464/